

Generation of Energy Efficient Trajectories for NIMS3D, a Three-Dimensional Cabled Robot

Per Henrik Borgstrom*, Nils Peter Borgstrom*, Michael J. Stealey*, Brett Jordan*, Gaurav S. Sukhatme**,
Maxim A. Batalin* and William J. Kaiser*

Abstract—In this paper we describe an algorithm to generate energy efficient trajectories for NIMS3D, a three-dimensional cabled robotic platform. Optimized parabolic paths are used to exploit the relatively low I^2R loss associated with operation in lower regions of the workspace. Trajectory optimization is sufficiently fast to enable real time operation. Experimental results on a physical system for a three cable deployment show substantial reductions in energy consumption as compared to linear trajectories.

I. INTRODUCTION

Cable driven robots consist of computer driven actuators that enable controlled release of cables. These cables, in turn, may support a wide range of end-effector systems. The actuators can be stationary or mobile, and are positioned in the extremities of the robot workspace. The range of the end-effector is limited to the volume or plane defined by these actuators, although, in general, stability concerns further limit the range of operation.

The authors of [1] describe several advantages of cabled robots, including:

- 1) Remote location of motors and controls
- 2) Rapid deployability
- 3) Potentially large workspaces
- 4) High load capacity
- 5) Reliability

Due to these characteristics, cabled robots are ideal for many tasks, such as handling of hazardous materials and disaster search and rescue efforts [2]. Additionally, several cabled robotic systems such as the SkyCam [3] and Cablecam [4] have found success in the fields of sports and entertainment. Similar platforms have been implemented for use as air vehicle simulators in development of sensing and control strategies [5].

In [6], we introduced a novel cabled robot - NIMS3D. Fig. 1 shows a schematic diagram of NIMS3D. The system is comprised of three components: 1. the infrastructure, consisting of poles and pulleys; 2. a generic node platform, on which a variety of sensors can be mounted; 3. the motor control box, which controls the spooling of the suspension cables. The

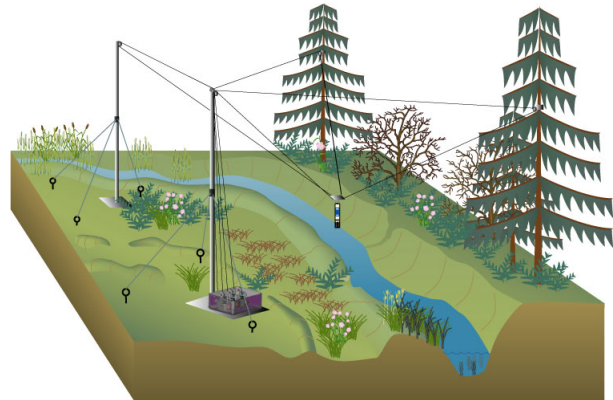


Fig. 1. A Schematic of NIMS3D

cables, which are non-elastic, low-mass, high tensile strength fishing line, all originate from a single motor-control box and connect to the node platform via pulleys. By virtue of this common origin, all cables, controllers, motors and power requirements are isolated to a single area of the deployment site. This allows for easy access to all wired components and enables flexibility in deployment configurations. While the first generation of NIMS3D consisted of a three cable configuration, fabrication of a four cable system with tension control capabilities is currently underway.

One of the shortcomings of cabled robotic platforms such as NIMS3D is that the weight of the end-effector must be supported by cables whose vertical angle is often quite shallow. This can result in very high cable tensions, particularly if the end-effector is to operate in the upper regions of the workspace. Because actuator torque and armature current are linearly related [7], high cable tensions result in high currents, which cause large Ohmic I^2R losses and, consequently, excessive power dissipation in the motors. For remote deployments where no power grid is available, this might significantly reduce deployment lifetime. Additionally, industrial robots might incur high operating costs due to poor efficiency.

There is much previous work in trajectory generation for parallel manipulators. The authors of [8] describe generation of time-minimal trajectories for six degree-of-freedom parallel configurations, whereas [9] describes trajectory generation for cable based parallel manipulators. Much of this prior work aims to minimize time of execution of a desired trajectory, which often adversely affects energy efficiency.

This work was supported by the US National Science Foundation (NSF) under Grants ANI-00331481, CCR-0120778, and IIS-0133947

Per Henrik Borgstrom is a graduate student in the Department of Electrical Engineering, University of California, Los Angeles, Los Angeles, CA 90095, USA henrik@ee.ucla.edu

* Department of Electrical Engineering at UCLA

** Department of Computer Science at USC

All authors are affiliated with the Center for Embedded Networked Sensing (CENS)

The problem that this paper addresses is as follows: Given a starting location and a desired destination in an unobstructed NIMS3D workspace, how might nonlinear trajectories be utilized to improve overall efficiency and reduce I^2R loss in the actuators? The generation of these optimized trajectories must be computationally inexpensive, allowing for real-time operation. There are no constraints on the duration of the trajectory, although the speed of the end-effector must not exceed a velocity limit given by V_{max} . The presented solution is to use optimized parabolic trajectories to exploit regions of the workspace characterized by low cable tension. Computing the energy-optimal parabolic trajectory requires a straightforward optimization across a single variable, resulting in fast computation time.

The remainder of this paper is structured as follows: In Section II, properties of actuators used in our experiments are discussed. In Section III, the method used to predict the I^2R energy loss of a given parabolic trajectory is described, and, thereafter, we describe the methods used to compute the optimal parabolic trajectory. In Section IV, experimental results are provided that show improved energy efficiency for a typical set of trajectories. Furthermore, the relative improvement is consistent with that predicted by simulations. In Section V, we conclude and offer a number of future research goals.

II. ACTUATOR MODELING

In order to enable improved energy efficiency in a cabled robotic system, it is important to generate a valid model for its actuator systems. The actuators in our robot are brushed DC gearmotors that are driven by means of PWM controlled H-bridges [10]. DC motors are governed by the equations given in (1) and (2) [7].

$$V(t) = L \frac{\partial I(t)}{\partial t} + RI(t) + K_E \omega \quad (1)$$

$$\tau(t) = K_T I(t) \quad (2)$$

where $V(t)$ is the applied voltage, $I(t)$ is actuator current, L and R are the armature inductance and resistance respectively, τ is torque, ω is motor speed, and K_T and K_E are motor constants, which, in SI units, are equal. In this paper, a quasi static approximation is made and time derivatives are taken to be zero. Therefore, after dropping the $L \frac{\partial I(t)}{\partial t}$ term, we proceed by rearranging (1), substituting (2), and multiplying both sides by I , which yields:

$$VI = \tau\omega + I^2R = \tau\omega + IR \frac{\tau}{K_T} \quad (3)$$

where VI is electrical power, $\tau\omega$ is power delivered to the load, and I^2R is loss in the armature resistance. Motor efficiency is therefore given by:

$$\frac{\omega}{\omega + \frac{IR}{K_T}} \quad (4)$$

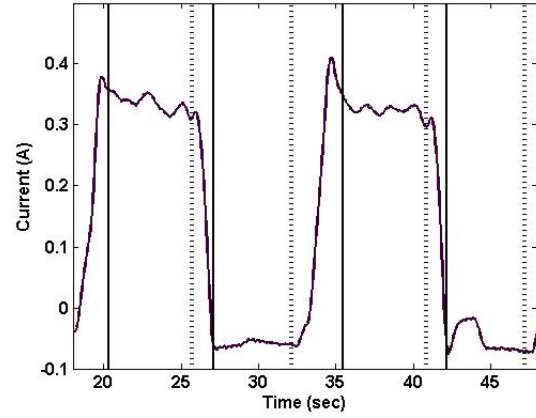


Fig. 2. Motor current during two cycles of raising and lowering of a 1kg load. The solid and dotted lines indicate starting and ending times for current averaging.

It is apparent from (4) that motor efficiency increases with ω . Thus, if acceleration and deceleration costs are ignored, operating actuators at full speed improves efficiency.

While this formulation does yield an important result, the motors considered are ideal and are not affected by non linearities such as friction. The motors used in NIMS3D are heavily geared to enable improved weight capacity, and these gearboxes cause a substantial amount of friction. In order to characterize the current response of the actuators to various velocities and torques, a precision 50m Ω high-side current sense resistor was placed in series with each motor. The voltage across this resistance is magnified by a differential amplifier [11] and thereafter low-pass filtered to remove high-frequency effects caused by PWM noise and brushed commutation. The resulting signals are sampled via 16-bit ADC circuits produced by Burr-Brown [12]. Thereafter, each motor is commanded to raise and lower loads with varying masses at increasing velocities. For these experiments, each cable supports its own load and raises it vertically. Thus, if velocity is constant, the tension in the cable is equal to the weight of the load and is thereby directly related to motor torque. The measured signals for two cycles of one such experiment are shown in Fig. 2. Average motor current is recorded for each velocity and mass. Transient current spikes associated with initial acceleration are evident, but because of the quasistatic nature of NIMS3D trajectories, these peaks are excluded from the computation of average current, and the averaging includes only those values between the start and end times indicated by solid and dotted vertical lines respectively.

The current values associated with each velocity and mass for each motor are stored in lookup tables. One such table is plotted in Fig. 3. This plot reveals that the relationship between current and cable tension is not at all linear. However, it is evident that there are two distinct regions defined by linear current-tension relationships. One corresponds to lifting a mass against gravity, and the other corresponds to lowering

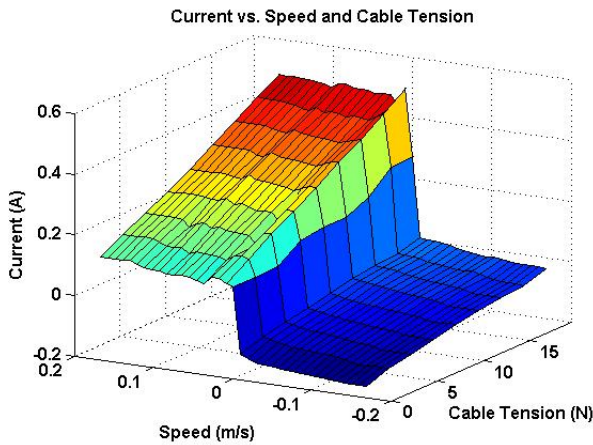


Fig. 3. Motor current shown as a function of velocity and cable tension

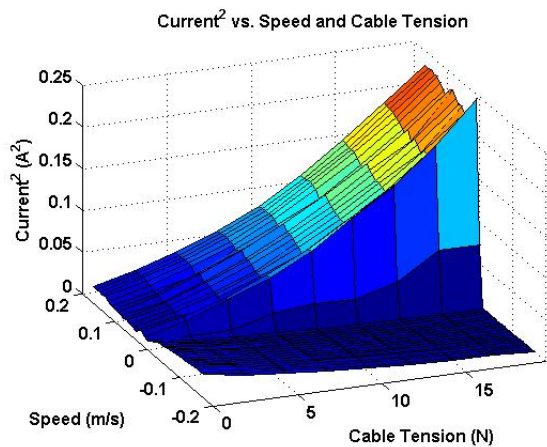


Fig. 4. The square of motor current shown as a function of velocity and cable tension

it. A plot of the square of these current values, shown in Fig. 4, is somewhat more meaningful, as the primary source of inefficiency in DC motors is I^2R loss. This plot reveals (1) a quadratic relationship between power loss and tension in raising a load and (2) negligible levels of power loss in lowering a load. These motor models are subsequently used in creating optimized parabolic trajectories.

III. PARABOLIC TRAJECTORY GENERATION

Operating in the upper regions of the workspace results in high cable tensions and low efficiency. Thus, it may be desirable to exploit the lower tensions and reduced Ohmic loss associated with the nether regions of the workspace. This is enabled by using downward parabolic trajectories which reduce operation in the undesirable upper regions of the workspace.

A. Calculating the Cost of Parabolic Trajectories

In generating a parabolic trajectory, an appropriate shift and rotation of coordinates is employed such that the starting point is at the origin and the destination lies at some point

$(x_f, 0, z_f)$, in a temporary coordinate system defined as $\hat{x}, \hat{y}, \hat{z}$. A trajectory can be defined as in (5).

$$\hat{z} = A\hat{x}^2 + B\hat{x} + C \quad (5)$$

where A , B , and C are parameters determining the shape of the parabola. At the origin of the temporary coordinate system, $\hat{x} = 0$ and $\hat{z} = 0$, so C must also be 0. We also have that $z_f = Ax_f^2 + Bx_f$, which yields:

$$B = \frac{z_f - ax_f^2}{x_f} \quad (6)$$

Thus, the trajectory can be completely defined by a single parameter, which is advantageous in subsequent optimizations.

Clearly, a parabolic path between two points is longer than the corresponding linear path. Because node velocity can not exceed V_{max} , the velocity limit of the system, the parabolic path incurs delays in completing the desired move. The relative increase in distance is small for moderate values of A , but as A grows, the distance penalty increases, and it is this distance penalty that ultimately limits the extent to which optimized trajectories exploit lower regions of the workspace.

In order to derive expressions for motor velocities, we begin by introducing the velocity kinematics of the platform, which are described in [13]. The inverse jacobian matrix J , consists of three rows which are the unit vectors directed from each of the pulleys to the node.

$$\dot{L} = \begin{bmatrix} \dot{L}_1 \\ \dot{L}_2 \\ \dot{L}_3 \end{bmatrix} = \begin{bmatrix} \vec{l}_1^T \\ \vec{l}_2^T \\ \vec{l}_3^T \end{bmatrix} \begin{bmatrix} \dot{x} \\ \dot{y} \\ \dot{z} \end{bmatrix} = J\vec{V} \quad (7)$$

where $[L_1 \ L_2 \ L_3]^T$ is the set of cable lengths, \vec{l}_i is the unit vector directed from the i^{th} pulley to the node, and \vec{V} is the time derivative of the node position $[x \ y \ z]^T$. The forward jacobian matrix F , can be found by inverting J , which is a full rank 3×3 matrix.

In order to compute cable tensions, we proceed as follows:

$$\sum_{i=1}^3 \vec{T}_i = m(\vec{a} - \vec{g}) \quad (8)$$

where m is node mass, $\vec{a} = \frac{\partial}{\partial t}\vec{V}$ is node acceleration, \vec{T}_i is the tension in the i^{th} cable. In addition, we have:

$$\sum_{i=1}^3 \vec{T}_i = - \begin{bmatrix} \vec{l}_1 & \vec{l}_2 & \vec{l}_3 \end{bmatrix} \begin{bmatrix} T_1 \\ T_2 \\ T_3 \end{bmatrix} = \Lambda \begin{bmatrix} T_1 \\ T_2 \\ T_3 \end{bmatrix} \quad (9)$$

where we note that $\Lambda = -J^T$. Combining (8) and (9) yields:

$$\begin{bmatrix} T_1 \\ T_2 \\ T_3 \end{bmatrix} = \Lambda^{-1}m(\vec{a} - \vec{g}) = -F^T m(\vec{a} - \vec{g}) \quad (10)$$

The expected current in the i^{th} motor at any point along the trajectory can be found by looking up in the empirical motor model the current value corresponding to the appropriate cable velocity, \dot{L}_i and tension, T_i . Thus, the total energy associated with a trajectory can be approximated by computing the integral of the square of this current over the duration of the trajectory and multiplying the result by R . The integration can be approximated to an acceptable level of accuracy by applying Simpson's rule with a small number N of points, since the parabolic trajectories are smooth and the resulting expected current values are well behaved. In practice, we have found that values of N near 10 are sufficient. It should be noted here that, in evaluating the cost of a trajectory, it is ascertained that the tensions in all cables remain between a lower and upper bound, T_{min} and T_{max} . The necessity of an upper bound is due to limits in maximum motor torque and cable tension, whereas a lower bound is required to maintain positive tension in all cables.

B. Parabolic Trajectory Optimization

As described in Section III-A, a parabolic trajectory can be defined by a single coefficient, A , which determines the amount of downward dip in a path. Large values result in large downward departures from a linear path and thereby low power operation, while small values remain close to the linear trajectory and are prone to the high power of operation in upper regions of the workspace. Thus, a reduction in trajectory costs is expected with increasing A . However, the increase in trajectory length corresponding to growing A causes the time to perform the trajectories to grow, and the lower average power of operation is ultimately offset by the longer integration period. The task then becomes to find A_{opt} , the positive, optimal value of A that results in the lowest expected energy cost. This bounded optimization is performed by means of an interior-reflective Newton method as described in [14] and [15]. Expected energy cost for a typical set of start and end points is shown plotted against A in Fig. 5. It is evident that, for this set of points, a trajectory defined by A_{opt} , which is near .27, will result in an I^2R reduction from 16.2J to 12.6J, a 22% improvement. In this case, the time penalty is roughly 13%. It should be noted that, while the metric that the optimization in this paper aims to minimize is I^2R loss, it could also be chosen as a weighted sum of I^2R loss and time, which allows for flexibility based on the time and energy constraints of a deployment.

IV. THREE CABLED EXPERIMENTAL RESULTS ON A PHYSICAL SYSTEM

In order to provide meaningful experimental results, NIMS3D was deployed in our lab and a set of representative start and endpoints was selected. The configuration parameters of the deployment are shown in Table I, and the start and endpoints of the experimental trajectories are shown in Table II. The set of trajectories maps out a roughly equilateral triangle with slight variations in height.

An experiment was performed in which straight line and optimized parabolic trajectories through the selected points

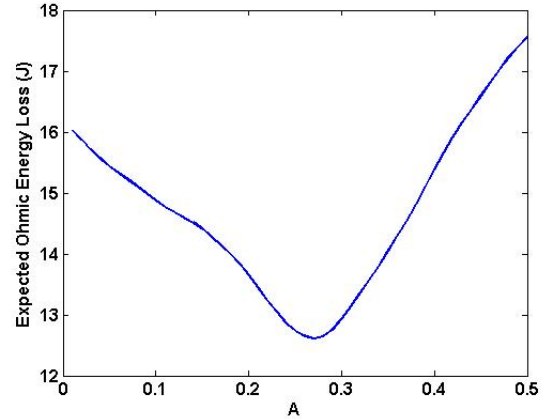


Fig. 5. Expected I^2R loss as a function of A

TABLE I
EXPERIMENTAL NIMS3D CONFIGURATION

Cable Origin	1	2	3
$x(m)$	3.96	0	8.46
$y(m)$	5.49	0	0
$z(m)$	3.1	2.36	2.77

TABLE II
EXPERIMENTAL TRAJECTORIES

Traj.	Start(m)	Dest(m)
1	$[6.00 \ 1.00 \ 1.70]^T$	$[4.25 \ 4.00 \ 2.10]^T$
2	$[4.25 \ 4.00 \ 2.10]^T$	$[2.50 \ 1.00 \ 1.70]^T$
3	$[2.50 \ 1.00 \ 1.70]^T$	$[6.00 \ 1.00 \ 1.70]^T$

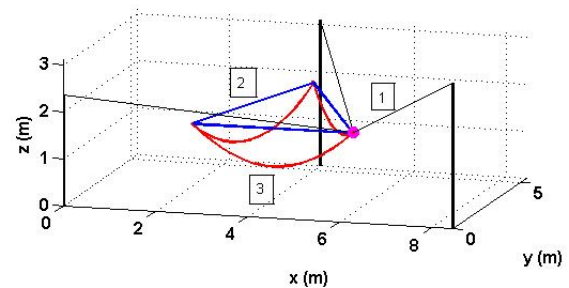


Fig. 6. Straight line and optimized parabolic trajectories through a set of test points

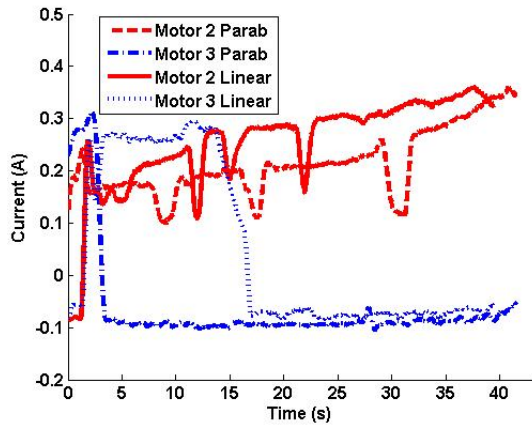


Fig. 7. Motor currents during execution of second path

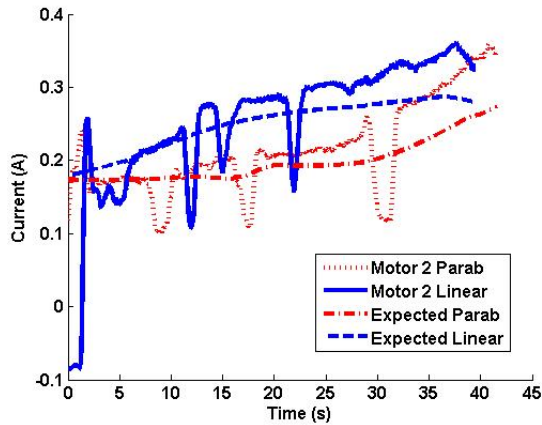


Fig. 8. Motor 2 current shown against expected values

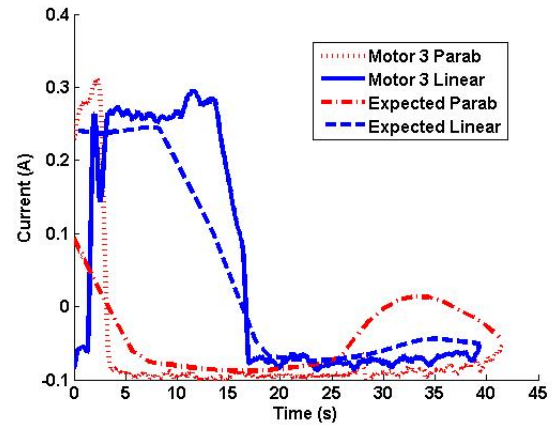


Fig. 9. Motor 3 current shown against expected values

TABLE III
ENERGY EFFICIENCY OF PARABOLIC TRAJECTORIES

Traj.	E_{Expect}	$E_{Expt.}$	T_{Ratio}	P_{Expect}	$P_{Expt.}$
1	.97	.95	1.03	.94	.92
2	.79	.69	1.15	.69	.60
3	.83	.78	1.13	.73	.69
Avg.	.86	.81	1.10	.79	.74

reduced more than total energy due to the longer execution time of parabolic paths. It should be noted that the relative improvement in energy efficiency that an optimized parabolic trajectory presents is highly dependent on system configuration and region of operation in the workspace. In upper regions of the workspace, which are characterized by very high cable tension and motor currents, slight downward deviations from linearity result in tremendous decreases in required actuator torque, whereas this effect is significantly reduced in lower regions of the workspace.

V. CONCLUSION

While cable array cranes such as NIMS3D present numerous advantages, one of the major disadvantages that has not been addressed in prior work is the potential for high actuator torque requirement and consequent high armature current. The resulting I^2R loss can result in poor actuator efficiency and high heat dissipation in the motors. In this paper, we have presented optimized parabolic trajectories that have been shown to significantly reduce I^2R loss in a set of typical trajectories. The optimization metric is readily adaptable to include time considerations, thereby allowing users to fine tune system performance. Results from experiments on a physical system and in simulations have been presented to verify the effectiveness of the proposed trajectories.

Current work is aimed at implementing a four cable NIMS3D system for aquatic applications. In the proposed system, the node floats in a body of water and is actuated by a set of four cables. While the parabolic trajectories described in this paper exploit the relative low power of operation in lower regions of the workspace, parabolic trajectories will be used in the aquatic system to exploit the low power

were executed and motor currents were sampled throughout the execution time. The experimental NIMS3D configuration and the resulting trajectories are shown in Fig. 6. Straight line paths are shown in blue, whereas parabolic paths are shown in red.

Currents for motors 2 and 3 are shown during linear and parabolic execution of the second path in Fig. 7. A trace of motor 1 current is omitted because it is near zero throughout the trajectory. Additionally, Figs 8 and 9 show currents for motors 2 and 3 respectively against the expected values. It is apparent that the experimental current values are in fair agreement with expected values and that there is a substantial decrease in average power. The intermittent dips in motor 2 current are most likely due to changes in the control effort resulting from slight trajectory overshoots.

The expected and experimentally observed reductions in I^2R loss for the three paths are shown in Table III, where E indicates the amount of I^2R energy loss in a parabolic trajectory relative to that in a linear path, T_{Ratio} indicates the relative time penalty, and P indicates the reduction of average power relative to a linear path. Average power is

characteristics of the middle of the workspace, where less cable tension is required to maintain stability. Additionally, we plan to generate motor models online by recording current data for the various velocities and tensions that the system encounters during operation. This data would then be used to complete a lookup table similar to the ones generated in Section II.

REFERENCES

- [1] A. Riechel, P. Bosscher, H. Lipkin, and I. Ebert-Uphoff, "Concept paper: Cable-driven robots for use in hazardous environments," in *Proceedings of the 10th International Topical Meeting on Robotics and Remote Systems for Hazardous Environments*, March 2004.
- [2] P. Bosscher, R. L. Williams, and M. Tummino, "A concept for rapidly-deployable cable robot search and rescue systems," in *Proceedings of ASME IDETC/CIE*, September 2005.
- [3] SkyCam. [Online]. Available: www.skycam.tv
- [4] CableCam. [Online]. Available: www.cablecam.com
- [5] K. Usher, G. Winstanley, P. Corke, D. Stauffacher, and R. Carnie, "Air vehicle simulator: an application for a cable array robot," in *IEEE International Conference on Robotics and Automation*, April 2005, pp. 2241–2246.
- [6] P. H. Borgstrom, M. Stealey, M. Batalin, and W. Kaiser, "Nims3d: A novel rapidly deployable robot for 3-dimensional applications," in *IEEE/RSJ International Conference on Intelligent Robots and Systems*, October 2006.
- [7] S. Cetinkunt, *Mechatronics*. John Wiley & Sons, Inc., 2007.
- [8] H. Abdellatif and B. Heimann, "Adapted time-optimal trajectory planning for parallel manipulators with full dynamic modelling," in *IEEE International Conference on Robotics and Automation*, April 2005, pp. 411–416.
- [9] M. Hiller, S. Fang, S. Mielczarek, R. Verhoeven, and D. Franitza, "Design, analysis and realization of tendon-based parallel manipulators," in *Mechanism and Machine Theory*, August 2004.
- [10] S. Cubed. [Online]. Available: <http://www.solutionscubed.com>
- [11] A. Devices. [Online]. Available: <http://www.analog.com/en/prod/0%2C2877%2CAD620%2C00.html>
- [12] Burr-Brown. [Online]. Available: <http://focus.ti.com/lit/ds/symlink/ads8321.pdf>
- [13] R. G. Roberts, T. Graham, and T. Lippitt, "On the inverse kinematics, statics, and fault tolerance of cable-suspended robots," vol. 15, no. 10, 1998.
- [14] T. Coleman and Y. Li, "On the convergence of reflective newton methods for large-scale nonlinear minimization subject to bounds," in *Mathematical Programming*, vol. 67, no. 2, 1994, pp. 189–224.
- [15] —, "An interior, trust region approach for nonlinear minimization subject to bounds," in *SIAM Journal on Optimization*, vol. 6, 1996, pp. 418–445.